

Strong Coupling between Microwave Photons and Nanomagnet Magnons

Justin T. Hou and Luqiao Liu

Department of Electrical Engineering and Computer Science, Massachusetts Institute of Technology, Cambridge, Massachusetts 02139, USA



(Received 4 March 2019; published 3 September 2019)

Coupled microwave photon-magnon hybrid systems offer promising applications by harnessing various magnon physics. At present, in order to realize high coupling strength between the two subsystems, bulky ferromagnets with large spin numbers are utilized, which limits their potential applications for scalable quantum information processing. By enhancing single spin coupling strength using lithographically defined superconducting resonators, we report high cooperativities between a resonator mode and a Kittel mode in nanometer thick Permalloy wires. The on-chip, lithographically scalable, and superconducting quantum circuit compatible design provides a direct route towards realizing hybrid quantum systems with nanomagnets, whose coupling strength can be precisely engineered and dynamic properties can be controlled by various mechanisms derived from spintronic studies.

DOI: 10.1103/PhysRevLett.123.107702

Hybrid quantum systems have been extensively studied to harness advantages of distinct physical systems and realize functions that cannot be achieved with any individual subsystem alone [1,2]. In particular, cavity and circuit quantum electrodynamics (cavity or circuit QED) [3–5] provide promising platforms for realizing hybrid quantum systems using Josephson qubits, mechanical systems [6], atoms [7], and quantum dots [8], as well as ensembles of spins [9,10]. For realizing coherent energy and information exchange, electric dipole interactions have been traditionally utilized to couple photons with other quantum excitations. Recently, coupled microwave photon-magnon systems have received great attention as an alternative approach to realize strong light-matter interactions using magnetic dipole coupling [11–17]. In this system, magnons in magnetic materials with high spin density are utilized, where coupling strength g is collectively enhanced by square root of number of spins ($g = g_s\sqrt{N}$) [14] to overcome the weak coupling strength g_s between individual spins and the microwave field. Along these lines, sizable ferrimagnets, yttrium iron garnet (YIG) with millimeter dimensions, have been employed for reaching strong coupling. While great success has been demonstrated in achieving coherent sensing and control over the magnonic quantum state using this architecture [18–20], one important question remains unanswered: whether such a system is scalable for achieving integrated hybrid quantum systems. In the meantime, reducing the size of magnets in this hybrid quantum system can potentially provide another degree of freedom for realizing active sensing and control of quantum states. In the study of spin electronics, sophisticated techniques have been developed for manipulating and detecting spin states using various electrical methods; however, these effects work efficiently only in nanoscale magnets [21–25]. In this

Letter, by utilizing lithographically defined superconducting resonators, we demonstrate strong magnon-photon coupling with a nanometer size Permalloy thin film stripe (Permalloy = Py = NiFe), where the number of spins is on the order of 10^{13} , 3 orders of magnitude lower than previous studies. The realization of magnon-photon coupled systems using metallic ferromagnets with conventional Si substrates demonstrates a highly engineerable and industrial compatible on-chip device design. Moreover, the large coupling strength with nanomagnets provides a direct avenue towards scalable hybrid quantum systems which can benefit from various magnon physics, including non-linearity [26], synchronized coupling [27,28], and non-Hermitian physics [29,30], as well as current or voltage controlled magnetic dynamics [21–25].

Figure 1(a) shows the image of a typical lithographically defined Nb superconducting coplanar waveguide (CPW) resonator that is coupled with a thin film ferromagnet (inset). We can model this hybrid system quantum mechanically as a macrospin coupled to an LC resonator through oscillating magnetic field \mathbf{b}_{rf} generated by the inductor, where $\mathbf{b}_{\text{rf}} = b_{\text{rf}}\hat{\mathbf{x}}$ is the magnetic field experienced by the macrospin per unit inductor current. During the experiment, an external field $\mathbf{B}_{\text{ext}} = -B_0\hat{\mathbf{z}}$ is applied to tune the intrinsic resonant frequency of the macrospin. The total Hamiltonian of the system can be written as [11,15,31]

$$\hat{H} = \hbar\omega_r \left(\hat{a}_r^\dagger \hat{a}_r + \frac{1}{2} \right) - \omega_m(B_0)\hat{S}_z + g_s(\hat{S}_+\hat{a}_r^\dagger + \hat{S}_-\hat{a}_r), \quad (1)$$

where \hat{a}_r^\dagger (\hat{a}_r) is the creation (annihilation) operator of microwave photon modes in the resonator, and $\hat{\mathbf{S}} = \frac{1}{2}(\hat{S}_+ + \hat{S}_-)\hat{\mathbf{x}} + \frac{1}{2i}(\hat{S}_+ - \hat{S}_-)\hat{\mathbf{y}} + \hat{S}_z\hat{\mathbf{z}}$ is the macrospin operator,

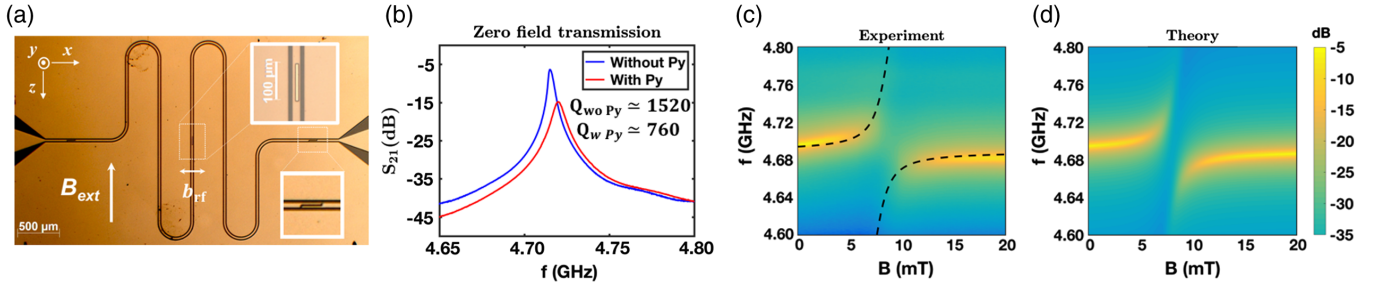


FIG. 1. (a) Photo of a CPW resonator device with $100 \mu\text{m} \times 8 \mu\text{m} \times 50 \text{ nm}$ MgO/Py/Pt stripe deposited at the center of the signal line. The distance $l = 12 \text{ mm}$ between the two open gaps at the ends of signal line defines the fundamental resonant frequency to be 4.96 GHz . (b) Microwave transmissions at 1.5 K with zero applied field before and after Py is deposited, exhibiting resonance signals with quality factors 1570 and 760 , respectively. With Py, the resonator mode is blue detuned due to residual coupling to the magnon mode. (c) Microwave transmission as a function of frequency and in-plane magnetic field at 1.5 K for a sample with $500 \mu\text{m} \times 8 \mu\text{m} \times 50 \text{ nm}$ Py showing the characteristic anticrossing of magnon-photon coupling. [The data from (b) and (c) are taken from different samples.] (d) Theoretical microwave transmission spectrum calculated using input-output theory with parameters obtained from the experiment.

with \hat{S}_+ (\hat{S}_-) raising (lowering) the z component of the macrospin. The resonant frequencies of the resonator ω_r and the macrospin $\omega_m(B_0)$ are given by $\omega_r = 1/\sqrt{LC}$ and the Kittel formula, separately. The coupling strength between photons and individual spins in the magnetic material g_s can be represented as $g_s = g_e \mu_B b_{\text{rf}} \omega_r / \sqrt{8\hbar Z_r}$ [31,33], with $Z_r = \sqrt{L/C}$ being the characteristic impedance of the LC resonator. The eigenfrequencies of the hybrid system can be calculated as [12]

$$\omega_{\pm} = \omega_r + \Delta/2 \pm \sqrt{\Delta^2 + 4g^2/2}, \quad (2)$$

where $\Delta = \omega_m(B_0) - \omega_r$ is the detuning and $g = g_s \sqrt{N}$ is the total magnon-photon coupling strength [31]. Therefore, in order to achieve scalable strong magnon-photon coupling with reduced N , it is important to increase the value of g_s . For a fixed resonant frequency of the resonator, two strategies can be employed to achieve this: (i) increasing b_{rf} by adjusting geometry of the inductive wire, or by placing the magnet close to the location with maximum magnetic field in the resonator; (ii) reducing Z_r by utilizing low-impedance resonators with small L and large C . Adopting the first strategy in a superconducting CPW resonator, we first realize a relatively high $g_s^{\text{CPW}}/2\pi = 18 \text{ Hz}$ by depositing the Permalloy stripe directly on top of the signal line with a thin insulating insertion, where strong coupling is realized with as few as 10^{13} spins. Furthermore, by combining both strategies, we show that very high coupling $g_s^{\text{LE}}/2\pi = 263 \text{ Hz}$ can be achieved in a lumped element LC resonator, which allows another 2 order of magnitude reduction in spin number N to achieve similar coupling strength.

To enhance the microwave magnetic field generated by unit inductor current b_{rf} , we minimize the width of the CPW resonator signal line in Fig. 1(a) to be $w^{\text{CPW}} = 20 \mu\text{m}$. The $l = 12 \text{ mm}$ long resonator is then capacitively coupled to

the external circuit through two gaps at the ends of signal line, leading to a fundamental resonant frequency $\omega_r/2\pi = c/2l\sqrt{\epsilon_{\text{eff}}} \approx 4.96 \text{ GHz}$, where c is the speed of light and $\epsilon_{\text{eff}} = 6.35$ represents the average dielectric constant of the vacuum and Si substrate [34]. The fundamental mode has a current distribution which reaches maximum at the center of the signal line, where we deposit a MgO(5 nm)/Py(50 nm)/Pt(10 nm) stripe by magnetron sputtering followed by lift-off. The thin insulating MgO layer protects superconducting Nb from ferromagnetic exchange coupling, while bringing Py close to the surface of Nb for large rf magnetic field. We mount the device in a cryostat with a base temperature of 1.5 K and study the transmission of microwave signal with a vector network analyzer. The transmission of the resonator before and after the deposition of Py stripe at zero field is shown in Fig. 1(b), where the quality factor can be determined to be $Q = 1570$ and 760 separately. To tune the frequency of magnetic resonance, an in-plane magnetic field \mathbf{B}_{ext} is applied along the long axis direction of Py stripe. As the rf magnetic field produced by the signal line is perpendicular to the external field direction, the ferromagnetic resonance (FMR) mode can be excited, thereby inducing a microwave photon-magnon coupling. Figure 1(c) shows the transmission of a sample with $500 \mu\text{m} \times 8 \mu\text{m}$ lateral dimensions as a function of frequency and applied magnetic field. The distinct anticrossing feature at $B_0 = 8 \text{ mT}$ is a result of microwave photon-magnon coupling where interaction between the two modes lifts the degeneracy in resonance frequencies. The resonant modes evolution can be fitted by Eq. (2), with $\omega_m(B_0) = \gamma \sqrt{[B_0 + (N_y - N_z)\mu_0 M_s][B_0 + (N_x - N_z)\mu_0 M_s]}$ given by the Kittel formula, where $\gamma/2\pi \approx 28 \text{ GHz/T}$ is the gyromagnetic ratio. In $\omega_m(B_0)$, the demagnetization factors N_i are taken into account, which can be analytically calculated with the dimension of the Py stripe [35].

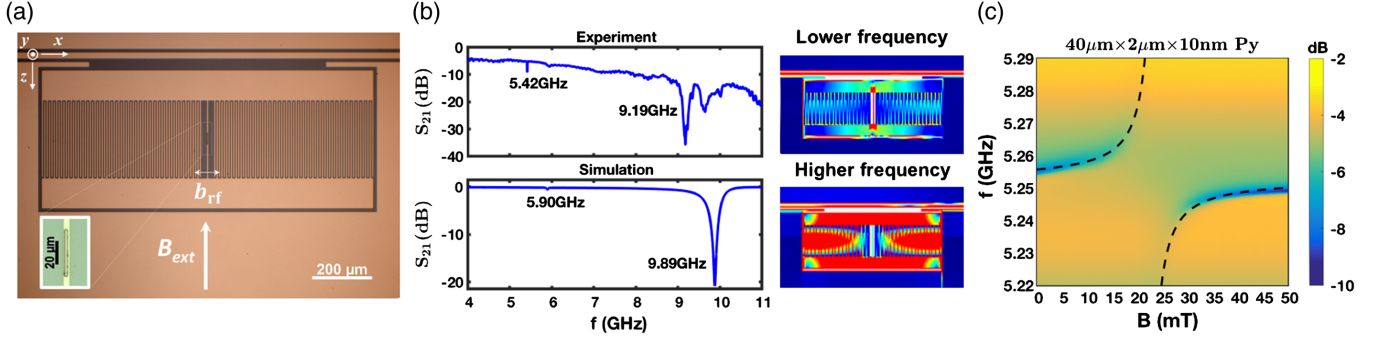


FIG. 2. (a) Image of a low-impedance lumped element resonator device with $40 \mu\text{m} \times 2 \mu\text{m} \times 10 \text{ nm}$ MgO/Py/Ta stripe deposited at the center of the $4 \mu\text{m}$ wide inductive wire. (b) (Left panels) Microwave transmission of the low-impedance resonator obtained from experiment and simulation. Two modes are observed as transmission minima due to photon absorption from the signal line. (Right panels) Simulation of current density distribution of the resonant modes, respectively. Red and blue areas indicate regions with strong and weak current densities, respectively. The first harmonic mode exhibits large current density at the central inductive wire which enhances coupling. (c) Microwave transmission as a function of frequency and in-plane magnetic field at 1.5 K. $\mu_0 M_s = 1.1 \text{ T}$ and $g/2\pi = 74.5 \text{ MHz}$ are determined from the fitting shown in dashed line. Minimum transmission shows up under resonant conditions.

Through the fitting, we extract the coupling strength $g/2\pi = 64 \text{ MHz}$, the saturation magnetization $\mu_0 M_s = 1.2 \text{ T}$ of the Py stripe, and the resonator frequency $\omega_r^{\text{CPW}}/2\pi = 4.690 \text{ GHz}$. Furthermore, we obtain the decay rates of the resonator mode $\kappa_r/2\pi = 1.5 \text{ MHz}$ and magnon mode $\kappa_m/2\pi = 122 \text{ MHz}$ by a transmission measurement of bare resonators and an independent FMR measurement of Py(50 nm)/Pt(10 nm) bilayer separately. To validate the coupling strength and decay rates, we adopt the input-output theory, which gives the microwave transmission coefficient as a function of frequency and magnetic field in our system [12,36]:

$$S_{21}(\omega, B_0) = \frac{\kappa_{r,\text{ext}}}{i(\omega - \omega_r) - \kappa_r + \frac{g^2}{i[\omega - \omega_m(B_0)] - \kappa_m/2}}, \quad (3)$$

where $\kappa_{r,\text{ext}}$ describes the external coupling rate of the resonator and only results in a constant offset in units of decibel. With the parameters measured in our experiment, we plot the theoretical transmission spectrum in Fig. 1(d), which attains reasonable agreement with the experiment results, with the minimum transmission signal of the latter limited by the background level.

Using M_s and the magnetic volume of the Py stripe, we estimate the number of spins involved in the coupling to be $N = 2.1 \times 10^{13}$. By fabricating devices with different length of Py stripes, we confirm the scaling of $g \propto \sqrt{N}$ and extract $g_s^{\text{CPW}}/2\pi = 18 \text{ Hz}$ (Fig. 3). As the Py stripe is at the center of the $20 \mu\text{m}$ wide signal line, we can assume that the rf magnetic field is uniform throughout the Py volume and estimate $b_{\text{rf}}^{\text{CPW}} = \mu_0/2w^{\text{CPW}}$. Together with the designed impedance $Z_r^{\text{CPW}} \approx 50 \Omega$ of CPW resonators, we calculate the theoretical g_s to be $g_{s,\text{theory}}^{\text{CPW}}/2\pi = 14 \text{ Hz}$, which attains reasonable agreement with our experimental value. In the device with $2000 \mu\text{m}$ long Py, coupling

strength $g/2\pi = 171 \text{ MHz}$ is obtained, which is larger than κ_r and κ_m and therefore falls into the strong coupling region. The corresponding cooperativity $g^2/\kappa_r\kappa_m = 160$ is very high for this small magnetic volume.

Next, we adopt the strategy of impedance reduction to further enhance the coupling strength. Low-impedance lumped element LC resonator has recently been employed for paramagnetic electron spin resonance experiments [33,37,38], but the potential for reaching strong magnon-photon coupling remains largely unexplored. As is shown in Fig. 2(a), the resonator consists of large interdigitated capacitors in parallel with a small inductor and is capacitively side coupled to the signal line of a CPW. The measured transmission coefficient of this resonator is shown in Fig. 2(b), where a minimum transmission shows up under the resonant condition due to its absorptive nature, in contrast to transmission peaks observed in the CPW resonator. Two resonant modes are observed in the transmission of the bare resonator, with resonant frequencies located at 5.42 and 9.19 GHz separately. In order to understand the properties of the two modes, we carried out electromagnetic wave simulations (SONNET) and found that the lower frequency mode corresponds to the case with a high current density passing through the central inductive wire [see the simulation results in Fig. 2(b)]. We estimate the capacitance C of this mode analytically [39] to be 1.91 pF and obtain the corresponding inductance $L = 0.45 \text{ nH}$ using the measured ω_r . The characteristic impedance of this LC circuit is calculated to be $Z_r^{\text{LE}} = \sqrt{L/C} \approx 15.3 \Omega$, much smaller than the value of CPW resonators. Moreover, the inductor width w^{LE} is designed to be only $4 \mu\text{m}$ to further increase magnetic field intensity. Figure 2(c) shows the transmission of a resonator that is coupled with a $40 \mu\text{m} \times 2 \mu\text{m} \times 10 \text{ nm}$ Py wire, as a function of frequency and applied magnetic field. Fitting the resonant frequency evolution using Eq. (2), we extract

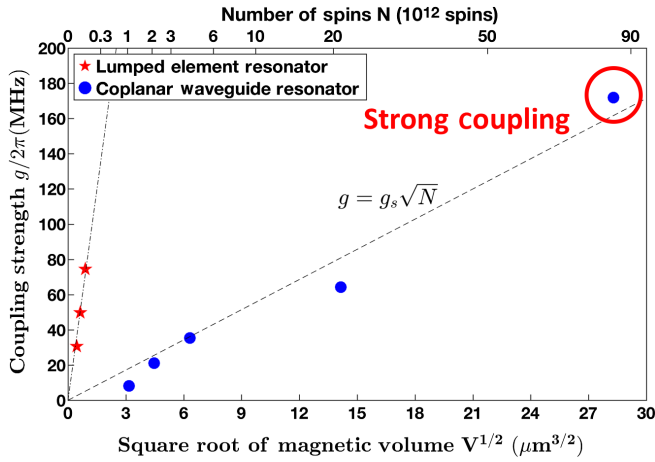


FIG. 3. Magnon-photon coupling strength g as a function of magnetic volume and spin number. The dashed lines represent fittings of the scaling rule $g = g_s\sqrt{N}$. The single spin coupling strength for two resonators in this Letter are determined to be $g_s^{\text{CPW}}/2\pi = 18$ Hz and $g_s^{\text{LE}}/2\pi = 263$ Hz in CPW resonators and lumped element resonators, respectively.

the coupling strength $g/2\pi = 74.5$ MHz, the saturation magnetization $\mu_0 M_s = 1.1$ T, and the resonator frequency $\omega_r^{\text{LE}}/2\pi = 5.253$ GHz. The relatively smaller M_s value compared with that of the previous CPW resonator sample comes from the thinner Py film thickness (10 vs 50 nm) and the potential magnetically dead interfacial layer [40]. With decay rates of the resonator mode $\kappa_r/2\pi = 1.05$ MHz and magnon mode $\kappa_m/2\pi = 122$ MHz, we calculate the cooperativity $g^2/\kappa_r\kappa_m = 43.3$, which is fairly large considering the very small number of spins ($N = 7.3 \times 10^{10}$). By fabricating devices with different lengths of Py stripes, we extract $g_s^{\text{LE}}/2\pi = 263$ Hz (Fig. 3), which is an order of magnitude larger than the value with the CPW resonator. The $g_s^{\text{LE}}/2\pi$ value obtained in our experiment is larger than the one calculated using our model $g_{s,\text{theory}}^{\text{LE}}/2\pi = 141$ Hz, which can be attributed to the enhancement of magnetic field at the edge of the inductor wire due to the field's nonuniform distribution [33,38]. The reasonable agreement between theoretical and experimental values in both CPW resonators and low-impedance lumped element resonators shows the usefulness of the formula $g = g_s\sqrt{N} = g_e\mu_B b_{\text{rf}}\omega_r\sqrt{N/8\hbar Z_r}$ obtained from our quantum mechanical model to predict magnon-photon coupling strength.

In summary, we demonstrate in this Letter high cooperativity microwave photon-magnon coupling between a resonator mode in planar superconducting resonators and a Kittel mode in Py nanomagnets. With enhanced g_s , the number of spins N involved for reaching strong coupling is 3 orders of magnitude lower than in previous experiments. In our experiment, a ferromagnetic metal with a relatively high damping coefficient (Py) is employed. By simply replacing magnetic metals with insulator thin films with ultralow damping such as YIG ($Q > 1000$) [41], we expect

strong magnon-photon coupling to be realized with as few as 10^7 spins using our current design. On the other hand, our studies show that the coupling strength obtained from the analytical model provides relatively precise estimate on the experimental values, which can be used as guidelines for a further scaling down of the magnonic system volume. For example, a lumped element resonator made by nanofabrication technique [42] with inductor width of ~ 100 nm can further enhance g_s by a factor of 40 and reduce the number of spins for reaching strong coupling using YIG to 10^4 . Our system is on chip, lithographically scalable [43], and circuit QED compatible, which demonstrates high potential for integrated hybrid quantum systems harnessing magnon physics. The demonstration of the coupled systems with ferromagnetic metal provides the opportunities to investigate magnon-photon coupling in a wide range of spintronic devices, such as magnetic tunnel junctions. Moreover, the high coupling strength with nanomagnets opens up the possibility of electrical control of the hybrid system dynamics utilizing spintronic effects, such as spin torque [21–25] and voltage controlled magnetic anisotropy [44].

This work is supported by the National Science Foundation under Grant No. ECCS-1653553, and AFOSR under Grant No. FA9550-19-1-0048.

Note added in proof.—Recently, a related paper by Li *et al.*, appeared [45]. They have also observed strong magnon-photon coupling using coplanar waveguide resonators.

- [1] Z.-L. Xiang, S. Ashhab, J. Q. You, and F. Nori, *Rev. Mod. Phys.* **85**, 623 (2013).
- [2] G. Kurizki, P. Bertet, Y. Kubo, K. Mlmer, D. Petrosyan, P. Rabl, and J. Schmiedmayer, *Proc. Natl. Acad. Sci. U.S.A.* **112**, 3866 (2015).
- [3] A. Wallraff, D. I. Schuster, A. Blais, L. Frunzio, R.-S. Huang, J. Majer, S. Kumar, S. M. Girvin, and R. J. Schoelkopf, *Nature (London)* **431**, 162 (2004).
- [4] R. J. Schoelkopf and S. M. Girvin, *Nature (London)* **451**, 664 (2008).
- [5] G. Wendin, *Rep. Prog. Phys.* **80**, 106001 (2017).
- [6] M. Aspelmeyer, T. J. Kippenberg, and F. Marquardt, *Rev. Mod. Phys.* **86**, 1391 (2014).
- [7] I. Buluta, S. Ashhab, and F. Nori, *Rep. Prog. Phys.* **74**, 104401 (2011).
- [8] K. D. Petersson, L. W. McFaul, M. D. Schroer, M. Jung, J. M. Taylor, A. A. Houck, and J. R. Petta, *Nature (London)* **490**, 380 (2012).
- [9] A. Imamolu, *Phys. Rev. Lett.* **102**, 083602 (2009).
- [10] D. I. Schuster, A. P. Sears, E. Ginossar, L. DiCarlo, L. Frunzio, J. J. L. Morton, H. Wu, G. A. D. Briggs, B. B. Buckley, D. D. Awschalom, and R. J. Schoelkopf, *Phys. Rev. Lett.* **105**, 140501 (2010).
- [11] Ö. O. Soykal and M. E. Flatt, *Phys. Rev. Lett.* **104**, 077202 (2010).

- [12] H. Huebl, C. W. Zollitsch, J. Lotze, F. Hocke, M. Greifenstein, A. Marx, R. Gross, and S. T. B. Goennenwein, *Phys. Rev. Lett.* **111**, 127003 (2013).
- [13] X. Zhang, C.-L. Zou, L. Jiang, and H. X. Tang, *Phys. Rev. Lett.* **113**, 156401 (2014).
- [14] Y. Tabuchi, S. Ishino, T. Ishikawa, R. Yamazaki, K. Usami, and Y. Nakamura, *Phys. Rev. Lett.* **113**, 083603 (2014).
- [15] M. Goryachev, W. G. Farr, D. L. Creedon, Y. Fan, M. Kostylev, and M. E. Tobar, *Phys. Rev. Applied* **2**, 054002 (2014).
- [16] L. Bai, M. Harder, Y. Chen, X. Fan, J. Xiao, and C.-M. Hu, *Phys. Rev. Lett.* **114**, 227201 (2015).
- [17] R. G. E. Morris, A. F. van Loo, S. Kosen, and A. D. Karenowska, *Sci. Rep.* **7**, 11511 (2017).
- [18] Y. Tabuchi, S. Ishino, A. Noguchi, T. Ishikawa, R. Yamazaki, K. Usami, and Y. Nakamura, *Science* **349**, 405 (2015).
- [19] X. Zhang, C.-L. Zou, N. Zhu, F. Marquardt, L. Jiang, and H. X. Tang, *Nat. Commun.* **6**, ncomms9914 (2015).
- [20] D. Lachance-Quirion, Y. Tabuchi, S. Ishino, A. Noguchi, T. Ishikawa, R. Yamazaki, and Y. Nakamura, *Sci. Adv.* **3**, e1603150 (2017).
- [21] S. I. Kiselev, J. C. Sankey, I. N. Krivorotov, N. C. Emley, R. J. Schoelkopf, R. A. Buhrman, and D. C. Ralph, *Nature (London)* **425**, 380 (2003).
- [22] K. Ando, S. Takahashi, K. Harii, K. Sasage, J. Ieda, S. Maekawa, and E. Saitoh, *Phys. Rev. Lett.* **101**, 036601 (2008).
- [23] V. E. Demidov, S. Urazhdin, H. Ulrichs, V. Tiberkevich, A. Slavin, D. Baither, G. Schmitz, and S. O. Demokritov, *Nat. Mater.* **11**, 1028 (2012).
- [24] L. Liu, C.-F. Pai, D. C. Ralph, and R. A. Buhrman, *Phys. Rev. Lett.* **109**, 186602 (2012).
- [25] Z. Duan, A. Smith, L. Yang, B. Youngblood, J. Lindner, V. E. Demidov, S. O. Demokritov, and I. N. Krivorotov, *Nat. Commun.* **5**, 5616 (2014).
- [26] Y.-P. Wang, G.-Q. Zhang, D. Zhang, T.-F. Li, C.-M. Hu, and J. You, *Phys. Rev. Lett.* **120**, 057202 (2018).
- [27] M. Harder, Y. Yang, B. Yao, C. Yu, J. Rao, Y. Gui, R. Stamps, and C.-M. Hu, *Phys. Rev. Lett.* **121**, 137203 (2018).
- [28] B. Zare Rameshti and G. E. W. Bauer, *Phys. Rev. B* **97**, 014419 (2018).
- [29] D. Zhang, J. Q. You, T.-F. Li, X.-Q. Luo, and Y.-P. Wang, *Nat. Commun.* **8**, 1368 (2017).
- [30] M. Harder, L. Bai, P. Hyde, and C.-M. Hu, *Phys. Rev. B* **95**, 214411 (2017).
- [31] See Supplemental Material at <http://link.aps.org/supplemental/10.1103/PhysRevLett.123.107702>, which includes Refs. [13,32], for an explanation of the Hamiltonian and a derivation of magnon-photon coupling strength.
- [32] M. H. Devoret, *Quantum Fluctuations in Electrical Circuits* (Elsevier, New York, 1997), p. 372.
- [33] C. Eichler, A. Sigillito, S. Lyon, and J. Petta, *Phys. Rev. Lett.* **118**, 037701 (2017).
- [34] M. Göppl, A. Fragner, M. Baur, R. Bianchetti, S. Filipp, J. M. Fink, P. J. Leek, G. Puebla, L. Steffen, and A. Wallraff, *J. Appl. Phys.* **104**, 113904 (2008).
- [35] A. Aharoni, *J. Appl. Phys.* **83**, 3432 (1998).
- [36] C. W. Gardiner and M. J. Collett, *Phys. Rev. A* **31**, 3761 (1985).
- [37] A. Bienfait, J. J. Pla, Y. Kubo, M. Stern, X. Zhou, C. C. Lo, C. D. Weis, T. Schenkel, M. L. W. Thewalt, D. Vion, D. Esteve, B. Julsgaard, K. Mlmer, J. J. L. Morton, and P. Bertet, *Nat. Nanotechnol.* **11**, 253 (2016).
- [38] A. Bienfait, J. J. Pla, Y. Kubo, X. Zhou, M. Stern, C. C. Lo, C. D. Weis, T. Schenkel, D. Vion, D. Esteve, J. J. L. Morton, and P. Bertet, *Nature (London)* **531**, 74 (2016).
- [39] R. Igreja and C. J. Dias, *Sens. Actuators A* **112**, 291 (2004).
- [40] K. Ounadjela, H. Lefakis, V. Speriosu, C. Hwang, and P. Alexopoulos, *J. Phys. (Paris), Colloq.* **49**, C8 (1988).
- [41] H. Chang, P. Li, W. Zhang, T. Liu, A. Hoffmann, L. Deng, and M. Wu, *IEEE Magn. Lett.* **5**, 1 (2014).
- [42] P. Haikka, Y. Kubo, A. Bienfait, P. Bertet, and K. Mlmer, *Phys. Rev. A* **95**, 022306 (2017).
- [43] K. Kakuyanagi, Y. Matsuzaki, C. Dprez, H. Toida, K. Semba, H. Yamaguchi, W. J. Munro, and S. Saito, *Phys. Rev. Lett.* **117**, 210503 (2016).
- [44] P. K. Amiri and K. L. Wang, *SPIN* **02**, 1240002 (2012).
- [45] Y. Liet *et al.*, preceding Letter, *Phys. Rev. Lett.* **123**, 107701 (2019).